ACS OMEGA

http://pubs.acs.org/journal/acsodf

Article

Magnetic Molecularly Imprinted Polymers for the Separation and Enrichment of Cannabidiol from Hemp Leaf Samples

Fan Yang, Dong Fu,* Peng Li, Xin Sui, Yang Xie, Jialong Chi, Jiaying Liu, and Bo Huang*

Cite This: *ACS Omega* 2023, 8, 1240−1248

Read Online

ACCESS | Metrics & More | Article Recommendations | Supporting Information

ABSTRACT: Cannabidiol (CBD) has attracted immense attention due to its excellent clinical effects in the treatment of various diseases. However, rapid and accurate extraction of CBD from hemp plant concentrates remains a challenge. Thus, novel magnetic molecularly imprinted polymers (CBD-MMIPs) with specific recognizing capability for CBD were synthesized using ethylene glycol dimethacrylate as the cross-linker, CBD as the template, methacrylic acid as the functional monomer, azobisisobutyronitrile as the initiator, and Fe_3O_4 nanoparticles modified with SiO_2 as the magnetic carrier. The morphological, magnetic, and adsorption properties of obtained CBD-MMIPs were characterized by scanning electron microscopy, transmission electron microscopy, X-ray diffraction, Fourier transform infrared spectroscopy, vibrating sample magnetometry, surface area and porosity analyses, and various adsorption experiments. The results showed that the CBD-MMIPs had selective specificity and high adsorption capacity for CBD. The adsorption of CBD by CBD-MMIPs could reach equilibrium in a short time (30 min), and the maximum adsorption capacity was as high as 26.51 mg/g. The specific recognition and selectivity properties of CBD-MMIPs to CBD were significantly higher than that of other structural analogues, and the regeneration tests established that the CBD-MMIPs had good recyclability. Furthermore, the CBD-MMIPs could be successfully used as an adsorbent to the extraction of CBD from hemp leaf sample concentrates with high recovery efficiencies (93.46−97.40%).

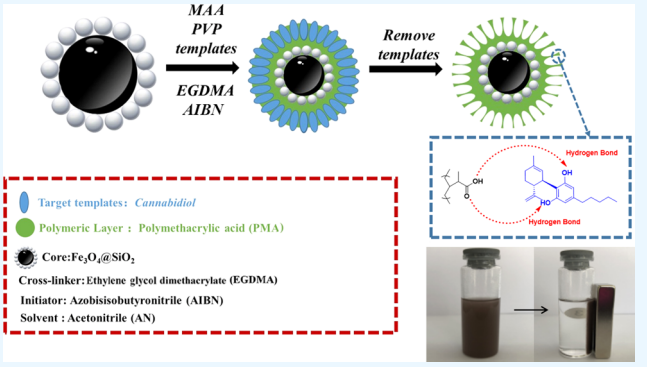

1. INTRODUCTION

Cannabidiol (CBD), a terpene phenol compound, is a nonpsychotropic cannabinoid found in Cannabis plants.[1] Initially, the function of CBD was found as an effective drug for Dravet syndrome in children. Many scientific studies demonstrate that CBD has multiple therapeutic effects, including neuroprotective, antiepileptic, anxiolytic, antipsychotic, anti-inflammatory, analgesic, and anticancer properties.[2−8] Nowadays, CBD has received immense attention due to the treatment or prevention COVID-19 and its complications.[9] Therefore, the realization of CBD mass production is very significant for the research and development of new drugs.

In general, CBD is prepared by chemical synthesis and plant extraction methods. Compared to chemical synthesis, the plant extraction method has several advantages, including lower cost, higher yield, and a simple preparation process. Up to now, several methods were used to extract CBD, such as the dynamic method (DM) of impregnation, ultrasonic-assisted extraction (UAE), microwave-assisted extraction (MAE), supercritical fluid extraction (SFE), and enzyme-assisted solvent extraction method.[10−12] Although the above methods can provide bulk CBD primary extracts, some disadvantages are also obvious, for instance, low selective adsorption for CBD, long extraction time, the large amount of organic chemical reagent consumption, and complex experimental conditions.[13,14] Thus, it is imperative to adopt a novel simple and rapid method for extracting and separating CBD from the real hemp samples.

Molecularly imprinted polymers (MIPs) were synthesized by molecular imprinting technology with specific recognition and selective adsorption of specific target molecules (template molecules) and their structural analogues. MIPs have many advantages: high selectivity, simple process, low operation cost, and fine reusability.[15−19] Recently, MIPs have received more and more attention from researchers and have been applied in chromatographic separation, solid-phase extraction, capillary electrophoresis, chemical sensors, mimic antibodies, and so on.[20−25]

Although MIPs have many advantages as described above, some disadvantages in some applications were obvious, such as low adsorption capacity, slow mass transfer rate, and

Received: October 15, 2022
Accepted: December 7, 2022
Published: December 19, 2022

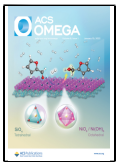

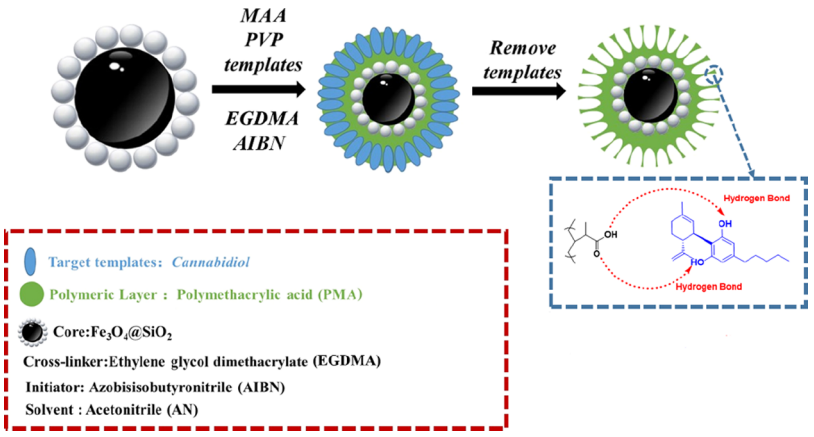

Figure 1. Schematic diagram for the synthetic process of CBD-MMIPs.

incomplete template elution. The surface molecular imprinting technique (i.e. all imprinted sites are generated directly on the surface of the MIPs) combined with magnetic separation technology is an ideal approach to solve these problems.[26−28] Magnetic molecularly imprinted polymers (MMIPs) can rapidly separate target molecules from sample solutions just under the condition of an external magnetic field.[29,30] In 2019, Xie et al. developed the photonic and magnetic dual-responsive protein MMIPs by surface polymerization, which could be applied to specifically recognize and extract bovine hemoglobin from actual biological samples.[31] In 2020, Cheng et al. reported that the MMIPs for effective extraction and determination of kaempferol from apple samples were successfully synthesized.[32] In 2022, Xie and co-workers fabricated novel magnetic and fluorescence-responsive MMIPs, which could be used to enrich and analyze glycoprotein in complex samples.[33] Therefore, MMIPs can be used as adsorptive materials for selective recognition and extraction of target molecules in different samples.[34−40] Based on the above considerations, we focused on the design and preparation of magnetic molecular imprinting material for the rapid separation of CBD from hemp leaf samples.

In this work, novel CBD-MMIPs with the specific recognizing capability for CBD were synthesized, and the imprinted polymers exhibited specific recognition, fast adsorption, and strong adsorption capacity for CBD. First, Fe_3O_4@SiO_2 magnetic carriers were prepared. Then, methacrylic acid (MAA), ethylene glycol dimethacrylate (EGDMA), CBD, and azobisisobutyronitrile (AIBN) were added to synthesizing CBD-MMIPs, and as-prepared CBD-MMIPs were characterized by several techniques, such as scanning electron microscopy (SEM), transmission electron microscopy (TEM), X-ray diffraction (XRD), Fourier transform infrared (FTIR) spectroscopy, vibrating sample magnetometry (VSM), and Brunauer−Emmett−Teller (BET) surface area and porosity analyses. Finally, the adsorption properties of the CBD-MMIPs were investigated by adsorption kinetics and adsorption isotherm experiments. The specific selectivity and reusability of CBD-MMIPs were researched using CBD and its similar structure molecules. Furthermore, the CBD-MMIPs could be used as a selective adsorbent for the extraction and separation of CBD from hemp leaf samples. It is worth noting that we prepared CBD-MMIPs by in situ polymerization directly using Fe_3O_4@SiO_2 as the magnetic core instead of using the vinyl-modified Fe_3O_4@SiO_2 or other functional groups (such as carbon−carbon double bonds, amino, etc.) reported in the literature.[34−44] The synthesis strategy was more simple and more convenient than other methods, and the synthesized molecularly imprinted polymers had a stronger selective adsorption capacity for the template molecules. To sum up, this novel CBD-MMIPs was a potential material for the rapid separation of CBD from hemp concentrates.

2. RESULTS AND DISCUSSION

2.1. Synthesis of CBD-MMIPs. The synthetic process of CBD-MMIPs is described in Figure 1. First, Fe_3O_4 nanoparticles were synthesized by the chemical coprecipitation method.[45] Then, to obtain magnetic particles with favorable chemical stability, good biocompatibility, and easy modification procedures by various groups, the surface of Fe_3O_4 nanoparticles was modified to obtain Fe_3O_4@SiO_2.[46] Subsequently, the CBD-MMIPs were fabricated from Fe_3O_4@SiO_2 by the surface-imprinted copolymerization method, in which CBD was used as the template molecule, EGDMA as the cross-linking agent, MAA as the functional monomer, AIBN as the initiator, and polyvinylpyrrolidone (PVP) as the dispersive reagent. Finally, the template molecules (CBD) were eluted to obtain the magnetic molecularly imprinted polymers with recognition sites and specially imprinted cavities. The molecularly nonimprinted polymers (MNIPs) were synthesized by the same procedure without CBD.

It was well known that the imprinting performance of the molecularly imprinted polymers greatly depended on the polymerization conditions. To obtain the excellent specific adsorption efficiency of CBD-MMIPs, several parameters (i.e., different solvents, the molar ratio of CBD to MAA, the ratio of MAA to EGDMA, and imprinting time) were optimized. The details of the results and discussion on the optimization of polymerization have been given in the Supporting Information (Figure S1).

2.2. Nitrogen Adsorption−Desorption Isotherm Analysis. The nitrogen adsorption−desorption isotherms and Barret−Joyner−Halenda (BJH) pore size distributions of CBD-MMIPs and MNIPs are shown in Figure S2, respectively. The specific surface area, average pore size, and pore volume are listed in Table S1. It could be seen from these results that the specific surface area of CBD-MMIPs calculated by the BET method is about 39.1 m^2/g, which was 8 times larger than that of MNIPs (4.9 m^2/g). The pore volumes of CBD-MMIPs and MNIPs were 0.08 and 0.009 cm^3/g, respectively. These results confirmed that CBD-MMIPs had a mesoporous structure,

https://doi.org/10.1021/acsomega.2c06649
ACS Omega 2023, 8, 1240−1248

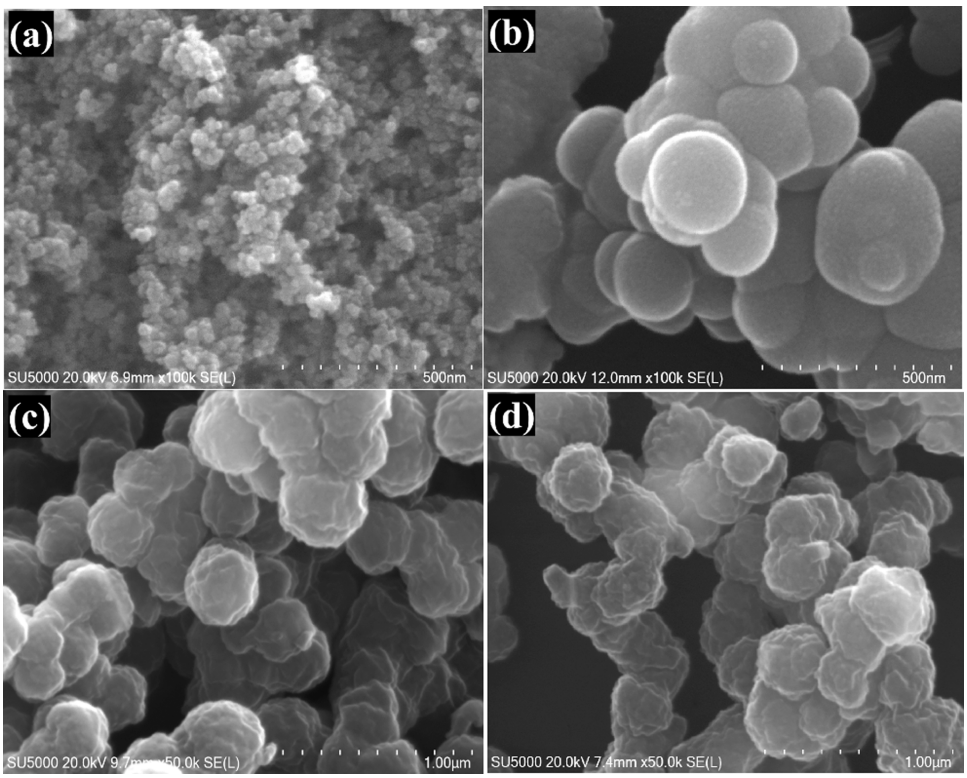

Figure 2. SEM images of Fe_3O_4 (a), Fe_3O_4@SiO_2 (b), CBD-MMIPs (c), and MNIPs (d) with the magnification of 100,000 (a, b) and 50,000 (c, d).

which also indicated the existence of molecular imprinting cavities.

2.3. SEM Analysis. The morphologies of Fe_3O_4 (a), Fe_3O_4@SiO_2 (b), CBD-MMIPs (c), and MNIPs (d) are shown in Figure 2. The Fe_3O_4 nanoparticles' diameter was around ∼15 nm with a regular spherical shape (Figure 2a). The particle size of Fe_3O_4@SiO_2 increased significantly, which was about 13 times that of Fe_3O_4 nanoparticles, and the formation of core−shell nanoparticles can be seen from the light and dark degrees (Figure 2b). As shown in Figure 2c,2d, the surface of Fe_3O_4@SiO_2 was coated with a polymeric layer of poly(methacrylic acid) (PMA), and both the shapes of the CBD-MMIPs and MNIPs were rougher than that of Fe_3O_4@SiO_2, which might be due to the cross-linking agent and functional monomers forming polymers on the surface of the Supporting Material. The average size of the CBD-MMIP microsphere was ∼380 nm with the CBD. The results proved that the CBD-MMIPs had been successfully synthesized, and the CBD molecules matched well with the imprinted cavities of CBD-MMIPs in the solution.

2.4. TEM Analysis. The TEM images of Fe_3O_4 (a), Fe_3O_4@SiO_2 (b), CBD-MMIPs (c), and MNIPs (d) are shown in Figure 3; the average diameters of Fe_3O_4, Fe_3O_4@SiO_2, CBD-MMIP, and MNIP nanoparticles were ∼15, ∼200, ∼380, and ∼400 nm, respectively. The particle size of Fe_3O_4 nanoparticles increased rapidly by modifying with SiO_2, and a relatively uniform coating layer was formed around the magnetic core, forming a relatively complete core−shell structure. The particle size of Fe_3O_4@SiO_2 nanoparticles increased further after being coated with a molecular imprinting layer with an imprinted film thickness of 185 nm. It is exciting to find that a multipoint blank spot was formed in the coating layer of CBD-MMIPs (Figure 3c), and the

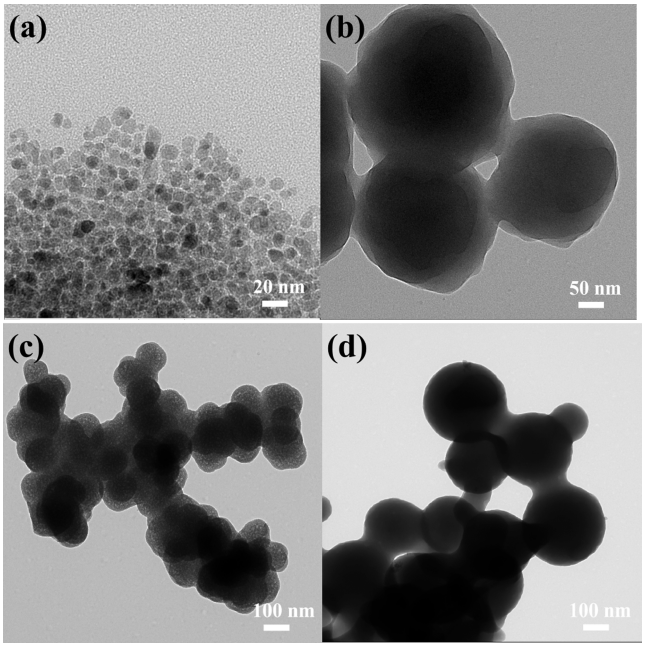

Figure 3. TEM images of Fe_3O_4 (a), Fe_3O_4@SiO_2 (b), CBD-MMIPs (c), and MNIPs (d).

obtained polymers layer had a thickness of about 180 nm, which illustrated that the binding sites almost existed on the surface of CBD-MMIPs, which indicates that the synthesis process of magnetic molecule-imprinted materials has achieved the expected purpose. The magnetic core−shell structure was formed, and the characteristic holes were formed in the molecule-imprinted layer.

https://doi.org/10.1021/acsomega.2c06649
ACS Omega 2023, 8, 1240−1248

2.5. FTIR Spectroscopic Analysis. The chemical composition of Fe_3O_4 (a), Fe_3O_4@SiO_2 (b), CBD-MMIPs (c), and MNIPs (d) was analyzed by FTIR spectroscopy (Figure S3). The strong adsorption at ∼590 cm^{-1} (a) is the characteristic peak for the stretching vibration of the Fe−O bond in Fe_3O_4 magnetic nanoparticles. The characteristic peaks at ∼1078 and ∼1124 cm^{-1} are the stretching vibration of the Si−O bond and Si−O−Si bond, respectively, indicating that a layer of SiO_2 is modified on the surface of Fe_3O_4 nanoparticles in Figure S3b−d. Figure S3c,d shows the peaks of C═O stretching vibration at ∼1709 cm^{-1} and C−H stretching vibration of the methyl group at ∼2932 cm^{-1}, indicating that the PMA layer was successfully formed on the surface of Fe_3O_4@SiO_2. In addition, CBD-MMIPs and MNIPs showed almost the same characteristic absorption bands due to the two polymers having similar skeletons.

2.6. XRD Analysis. XRD of Fe_3O_4 (a), Fe_3O_4@SiO_2 (b), CBD-MMIPs (c), and MNIPs (d) is displayed in Figure S4. For the four compounds mentioned above, six characteristic diffraction peaks for Fe_3O_4 have appeared in the 2θ range of 10−80° (i.e., 2θ = 29.89, 35.52, 43.16, 53.48, 57.26, 62.80°). The relevant 2θ value was indexed as (220), (311), (400), (422), (511), and (440), respectively, which were in accordance with the magnetite database of the JCPDS International Center (JCPDS Card: 19−629 for Fe_3O_4) file.[45] The results proved that all of the samples were composed of Fe_3O_4, and the crystal structures of Fe_3O_4 did not change during the polymerized process.

2.7. VSM Analysis. The magnetics of Fe_3O_4 (a), Fe_3O_4@SiO_2 (b), CBD-MMIPs (c), and MNIPs (d) were analyzed by VSM (Figure 4). There is no magnetic hysteresis in the four samples, and the coercivity and residual magnetization are almost 0, indicating that all of the compounds were superparamagnetic. For Fe_3O_4, Fe_3O_4@SiO_2, CBD-MMIPs, and MNIPs, the saturation magnetizations (M_s) are 49.69, 46.15, 42.08, and 39.82 emu/g, respectively. The value of magnetization decreased due to the shielding effect caused by the wrapping of the imprinted layer. However, the saturation magnetic induction intensity of CBD-MMIPs was still strong enough to quickly separate the polymers from the solution using a magnet. As shown in Figure 4B, CBD-MMIPs can be completely separated from the solution in only 10 s by the action of the external magnetic field. The results illustrated that the CBD-MMIPs processed excellent magnetic properties and can be applied to fast magnetic separation.

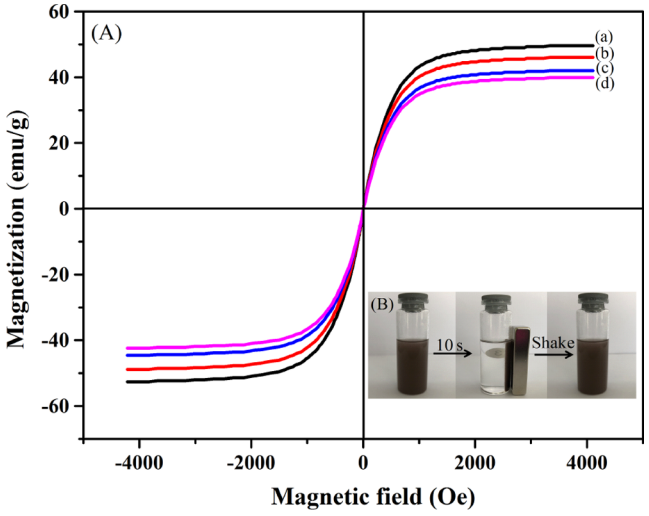

Figure 4. (A) Hysteresis loops of Fe_3O_4 (a), Fe_3O_4@SiO_2 (b), CBD-MMIPs (c), and MNIPs (d) at room temperature. (B) Magnetic response of CBD-MMIPs to an applied magnetic field.

2.8. Adsorption Kinetics. As shown in Figure S5, the adsorption capacities of CBD-MMIPs and MNIPs on CBD (10 mg/L) increased rapidly with the rising of adsorption time and almost reached adsorption equilibrium at about 30 min, while the adsorption rate and the adsorption capacities of CBD-MMIPs on CBD were always greater than those of MNIPs on CBD due to imprinting cavities and the specific adsorption sites that existed in CBD-MMIPs. The CBD molecules could be quickly entered into the imprinted cavities on the surface of CBD-MMIPs and retained in the cavities relatively stably through the formation of hydrogen bonds. However, the adsorption of CBD by MNIPs mainly relied on the nonspecific adsorption on the surface of MNIPs.

To further investigate the adsorption characteristics of CBD-MMIPs, the pseudo-first-order (eq 1) and pseudo-second-order (eq 2) kinetic adsorption models were used to fit the adsorption behavior of CBD-MMIPs and MNIPs. The nonlinear fitting formulas of the two models are as follows

$$q_t = q_e(1 - e^{-k_1 t}) \quad (1)$$

$$q_t = q_e^{\,2} k_2 t/(1 + q_e k) \quad (2)$$

where t is the time of adsorption, q_t is the adsorption capacity at t time, q_e is the equilibrium adsorption capacity, and k_1 and k_2 are the constants of the two equations. The results are displayed in Table S2 and Figure 5. By comparing the main parameter R^2, it is not difficult to find that the pseudo-first-order graph could better simulate the adsorption process of CBD-MMIPs and MNIPs. The calculated equilibrium adsorption capacity (27.33 mg/g) of CBD-MMIPs is close to that of the experimental result (26.51 mg/g).

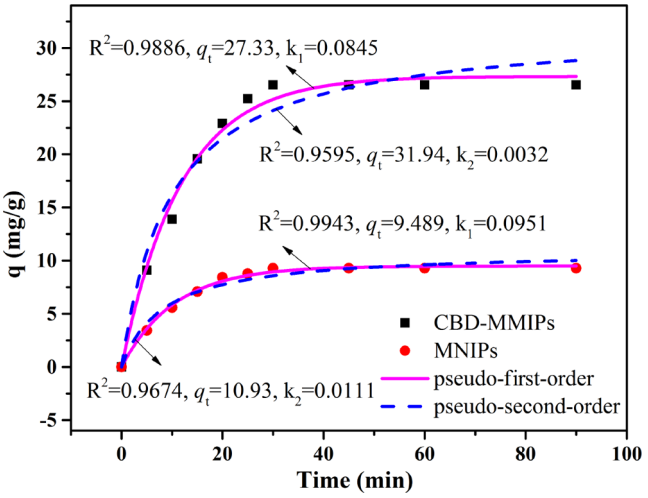

Figure 5. Pseudo-first-order plot and pseudo-second-order plot of adsorption kinetics for CBD-MMIPs and MNIPs.

2.9. Adsorption Isotherms. The isothermal adsorption experiments of CBD-MMIPs and MNIPs for CBD were investigated in different CBD concentrations ranging from 0.10−1.00 mg/L for 1 day at room temperature. As displayed in Figure S6, with the increase of the initial concentrations, the

https://doi.org/10.1021/acsomega.2c06649
ACS Omega 2023, 8, 1240−1248

adsorption capacity of CBD by CBD-MMIPs increased quickly as the concentration of CBD was below 6.00 mg/L and then increased slowly until reaching a saturated adsorption amount of 26.50 mg/g at 0.90 mg/L. The adsorption capacity of CBD by MNIPs also increased with the increase of the initial concentration and arrived an adsorption equilibrium of 9.61 mg/g at 0.90 mg/L. The results illustrated that the CBD recognition ability of CBD-MMIPs was higher than that of MNIPs and the maximum adsorption capacity of CBD by CBD-MMIPs was almost 3 times more than that of MNIPs (Figure S6), which is because of the existence of specific imprinted sites on the surface of CBD-MMIPs.

The models of Langmuir (eq 3) and Freundlich (eq 4) were used to fit the adsorption process of CBD by CBD-MMIPs and MNIPs, respectively. The nonlinear fitting formulas of the two models are as follows

$$q_e = q_m K_L C_e/(1 + K_L C_e) \quad (3)$$

$$q_e = K_F C_e^{1/n} \quad (4)$$

where q_m is the theoretical maximum adsorption capacity, q_e is the equilibrium adsorption capacity, C_e is the mass concentration of the solution at adsorption equilibrium, and K_L, K_F, and n are the adsorption constants of the two models, respectively.

The results are displayed in Table S3 and Figure 6. According to the Langmuir equation, the adsorption isotherm

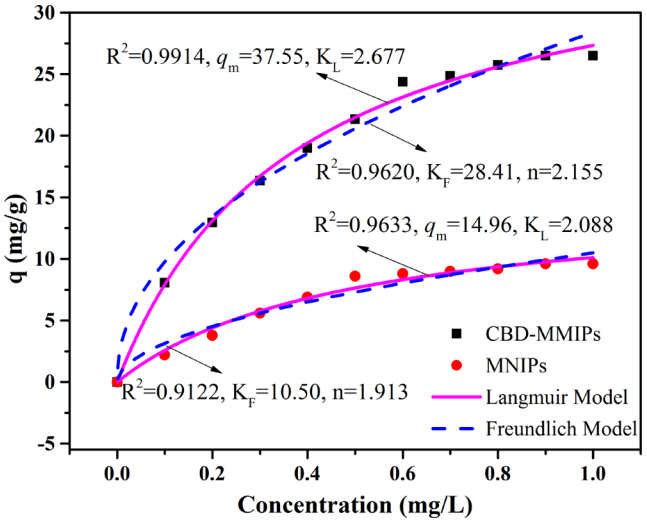

Figure 6. Langmuir adsorption model and Freundlich adsorption model for CBD-MMIPs and MNIPs.

parameters of CBD for CBD-MMIPs (R^2 = 0.9914) and MNIPs (R^2 = 0.9633) were higher than those of the Freundlich equation, indicating that the Langmuir model was more applicable for the CBD adsorption and the adsorption of CBD could be considered monolayer adsorption.

2.10. Selective Adsorption. To further investigate the selectivity of CBD-MMIPs to CBD, cannabinol (CBN), bisphenol A (BPA), and phenol were chosen as the interfering substance of competitive adsorption for their structures similar to CBD (Figure S7). As shown in Figure 7, due to the template-specific sites that existed on the surface of CBD-MMIPs, the adsorption capacity of CBD-MMIPs to CBD (25.57 mg/g) was significantly higher than those to CBN (9.60

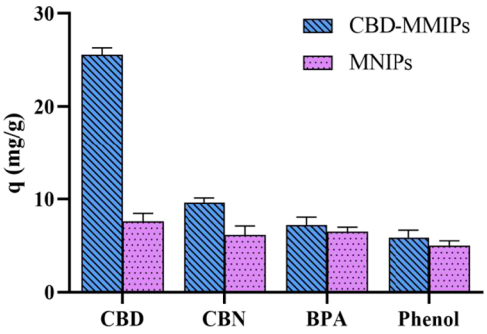

Figure 7. Selectivity of CBD-MMIPs and MNIPs for CBD, CBN, BPA, and phenol.

mg/g), BPA (7.20 mg/g), and phenol (5.86 mg/g). Meanwhile, the adsorption capacity of CBD-MMIPs to CBD was noticeably higher than that of MNIPs, on account of the imprinting recognition sites of CBD-MMIPs and the hydrogen bonding interactions between CBD and CBD-MMIPs. The poor adsorption capacity of MNIPs for the four compounds was due to the lack of specific recognition sites. In addition, the selectivity of CBD-MMIPs and MNIPs was evaluated by the imprinting factor (α) and selectivity factor (β); the equations are as follows

$$\alpha = q_{MMIPs}/q_{MNIPs} \quad (5)$$

$$\beta = \alpha_{CBD}/\alpha_M \quad (6)$$

where q_{MMIPs} and q_{MNIPs} are the adsorption capacity of CBD-MMIPs and MNIPs, respectively, and α_{CBD} and α_M are the imprinting factors for CBD and analogue, respectively. The imprinting factors of CBD, CBN, BPA, and phenol were 3.35, 1.56, 1.10, and 1.17, respectively. The selectivity factors of CBN, BPA, and phenol were 2.15, 3.04, and 2.86, respectively. The results proved again that the CBD-MMIPs had high specificity and selectivity for CBD compared to their structural analogues.

The competitive adsorption of the CBD-MMIPs and MNIPs to CBD was further studied. Figure S8 shows the competitive adsorption of CBD-MMIPs and MNIPs to CBD in the mixture solution of four substances. It could be seen that the adsorption capacity of CBD-MMIPs for CBD (16.86 mg/g) was noticeably higher than those for CBN (4.71 mg/g), BPA (3.25 mg/g), and phenol (3.14 mg/g). It was because the surface of CBD-MMIPs had sites that could selectively recognize and bind CBD. Notably, compared with the adsorption capacity of CBD-MMIPs in a single system (Figure 7), the adsorption capacity of CBD-MMIPs for each substance decreased in the multicomponent system mixed with CBD and their structural analogues (Figure S8). That might be due to the presence of interferents affecting the adsorption efficiency of CBD-MMIPs for CBD to a certain extent. Nonetheless, it could also be seen that the adsorption capacity of CBD-MMIPs to any substance was higher than the counterpart of MNIPs.

2.11. Reusability of CBD-MMIPs. Reusability is a crucial property for adsorbents. Thus, the reusability of the CBD-MMIPs and MNIPs was evaluated by measuring the adsorption capacity for CBD with nine adsorption−desorption cycles. As displayed in Figure S9, the adsorption capacities of CBD-MMIPs and MNIPs were reduced from 6.80 and 1.20 to 6.20 and 0.95 mg/g after nine regeneration cycles, respectively.

https://doi.org/10.1021/acsomega.2c06649
ACS Omega 2023, 8, 1240−1248

The resulting RSD values were 3.27 and 1.88%, respectively. The results indicated that CBD-MMIPs still maintained good stability after several adsorption−desorption cycles. The little decrease in adsorption might be due to the blockage and destruction of imprinted sites on the surface of CBD-MMIPs. The subtle change in the adsorption capacity of MNIPs was mainly because of the absence of the recognition sites for the selective adsorption of CBD on the surface of MNIPs. The results established that both CBD-MMIPs and MNIPs had good recyclability.

2.12. Optimization of Desorption Conditions. The desorption conditions were optimized by the selection of the elution solvent, the desorption time, and the amount of CBD-MMIPs. To determine the effect of different eluents, methanol, ethanol, petroleum ether, acetic acid/methanol (V/V = 2:8), and ethanol/acetonitrile (V/V = 2:1) were selected as eluents. As shown in Figure S10, when acetic acid/methanol (V/V = 2:8) was used as the elution solvent, the recovery efficiency of CBD was the highest, which could reach 94.43%, and it was significantly different from those of other elution solvents. Therefore, a mixture of acetic acid/methanol (V/V = 2:8) was adopted as the elution solvent.

The variation in the recovery efficiency of CBD on saturated CBD-MMIPs with desorption time can be seen in Figure S11. With the rising desorption time, the recovery efficiency of CBD increased continuously. The desorption reached equilibrium at 30 min, and the recovery efficiency of CBD was stable at about 94.30%. Thus, 30 min was selected as the optimum desorption time for CBD-MMIPs.

The effect of the amount of CBD-MMIPs on CBD recoveries is displayed in Figure S12. The recovery efficiency of CBD increased gradually with the increase of the amounts of CBD-MMIPs until its dosage reached 0.50 g (the recovery efficiency was about 94.60%), and then, the recovery efficiency was unchanged. Hence, the optimal dosage of CBD-MMIPs was 0.50 g.

2.13. Analysis of Hemp Leaf Samples. To further verify that CBD-MMIPs can be used for the enrichment and rapid separation of CBD from hemp extracting solution, the content of CBD in hemp leaf samples extracted by CBD-MMIPs was determined by high-performance liquid chromatography (HPLC) under the optimized experimental conditions. Figure 8a shows the chromatogram of the hemp leaf sample without CBD with the distribution of miscellaneous peaks between 2.81 and 3.22 min. Figure 8b shows the chromatogram of the hemp leaf sample spiked with standard CBD, which obviously appeared at 4.13 min. Figure 8c shows the chromatogram of the eluent after the enrichment of the spiked CBD with the CBD-MMIPs; the peak for CBD also appeared distinctly at 4.13 min, which was consistent with the retention time of CBD in the spiked sample solution. Other irrelevant compounds in the hemp leaf sample were eliminated. The results indicated that CBD-MMIPs could selectively adsorb CBD in the hemp leaf sample.

The linear range of the CBD concentration was 0.5−20 mg/L with a correlation coefficient of 0.9997. Signal-to-noise ratios (S/N) of 3 and 10 were used to determine the limit of detection (LOD) and the limit of quantification (LOQ). The values of LOD and LOQ were counted as 0.006 and 0.03 mg/L, respectively. The recovery, accuracy, and precision were detected through the standard addition method. It can be seen from Table 1 that the concentrations of CBD in the samples without adding standards ranged from 0.982 to 1.95 mg/L, the recoveries of standard addition ranged from 94.4 to 96.1%, and the relative standard deviation (RSD) ranged from 0.85 to 1.1%. The calculated intraday repeatability and interday reproducibility ranged from 2.2 to 4.1% and from 4.7 to 6.4%, respectively. The results demonstrated that CBD-MMIPs had high affinity, accuracy, and precision for CBD enrichment in the hemp leaf samples.

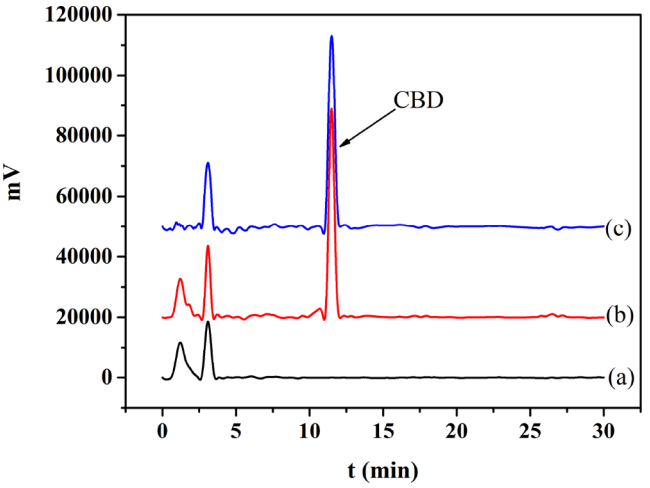

Figure 8. Chromatograms of the extracting solution of the hemp leaf sample (a), spiked sample solution of CBD at the concentration of 1.0 mg/L (b), and the elution of absorbed CBD-MMIPs (c).

Table 1. Recoveries and RSD for the Detection of CBD in Hemp Leaf Samples Using the CBD-MMIPs

					RSD (%, n = 3)	
sample	spiked levels (mg/L)	found levels (mg/L)	recovery (%)	RSD (%, n = 6)	intraday	interday
hemp leaf samples	1.04	0.982	94.4	1.6	3.4	5.8
	1.52	1.44	94.7	0.85	2.2	4.7
	2.03	1.95	96.1	1.1	4.1	6.4

A comparative study was also evaluated between our developed method and other reported methods for analyzing CBD, and the results are displayed in Table S4. Compared with previous CBD adsorption methods based on MIPs with different construction strategies, our resulting CBD-MMIPs had a greater adsorption capacity for CBD in the sample. Meanwhile, our method of preparation of CBD-MMIPs was easier and possesses higher selectivity than the reported MIP methods. Therefore, this proposed method based on the surface molecular imprinting technique could provide a rapid and convenient mode for the determination of CBD in hemp leaf samples.

3. CONCLUSIONS

In this work, novel CBD-MMIPs with special recognizing and selective adsorbing properties for CBD were synthesized by the surface molecular imprinting technique. The results exhibited that the CBD-MMIPs processed outstanding magnetic properties, rapid separating speed, high adsorption capacity, and excellent selectivity. The CBD-MMIPs just needed 30 min to reach the adsorption equilibrium with an improved imprinting capacity and a maximum adsorption amount of 26.51 mg/g. The adsorption kinetics and isotherm of the CBD-MMIPs and MNIPs were according to pseudo-first-order and the Langmuir

https://doi.org/10.1021/acsomega.2c06649
ACS Omega 2023, 8, 1240−1248

models, respectively. Selective adsorption and reusability experiments demonstrated that the CBD-MMIPs had a specific recognition ability for CBD and could be recycled nine times. The CBD-MMIPs were successfully applied to the selective separation and enrichment of CBD from hemp leaf samples and were easily collected using an external magnetic field, avoiding the steps of making packed columns as the traditional SPE, which might solve the defects of poor adsorption selection and low separation and purification efficiency of traditional separation technology.

4. EXPERIMENTAL SECTION

4.1. Reagents. Ferroferric oxide (Fe_3O_4) (98%), ferrous sulfate ($FeSO_4$) (99%), iron (III) chloride anhydrous ($FeCl_3$) (99%), azobisisobutyronitrile (AIBN) (99%), ethylene glycol dimethacrylate (EGDMA) (98%), polyvinylpyrrolidone (PVP) (98%), methacrylic acid (MAA) (98%), sodium hydroxide (NaOH) (99%), acetone (98%), methanol (98%), ethanol (99%), acetonitrile (99%), tetraethoxysilane (TEOS) (98%), tetrahydrofuran (99%), dichloromethane (99%), ammonium hydroxide (30%), oleic acid (99%), citric acid (99%), petroleum ether (99%). The reagents mentioned above are of analytical grade and purchased from Shanghai Aladdin Biochemical Technology Co., Ltd. CBD (96%), CBN (98%), BPA (99%), and phenol (99%) were purchased from Sinopharm Chemical Reagent Co., Ltd.

4.2. Instruments. The morphologies of the samples were observed using a transmission electron microscope (TEM, JEM-2100, Japan) and a scanning electron microscope (SEM, Hitachi SU5000, Japan). The structure characterization of samples was performed in the 4000−400 cm^{-1} range on an FTIR-7600 spectrometer (Lambda, Australia) (KBr pellet method). The crystal structure of the samples was measured using an X-ray diffractometer (XRD, X'Pert3 Powder, Netherlands). The magnetic properties of polymers were tested using a vibrating sample magnetometer (VSM-250, China). The BET surface area analysis was measured using a surface area and porosity analyzer (ASAP 2020 HD88). The analysis of adsorption experiments was performed using a high-performance liquid chromatograph (Agilent 1100) equipped with a diode array detection (DAD) system and a C_{18} analytical column (250 mm × 4.6 mm, 5.0 μm). The mobile phase consisted of methyl alcohol/water (V/V = 60:40) at a flow rate of 1.0 mL/min, and the sample injection volume was 20 μL.

4.3. Synthesis of Fe_3O_4 Nanoparticles. General procedure: 0.5 mol/L of $FeSO_4$ solution and 0.5 mol/L of $FeCl_3$ solution (V/V = 1:2) were mixed in a 250 mL three-neck flask. Then, 10 mL of NaOH solution (15 wt %) and 10 mL of oleic acid solution (10 wt %) were added to the mixture under a nitrogen atmosphere. The reaction system was heated at 70 °C for 1 h. After cooling down, the obtained Fe_3O_4 nanoparticles were separated using a magnet; the sediment was washed with deionized water at least five times and then dried under vacuum at 45 °C for 24 h.

4.4. Synthesis of Fe_3O_4@SiO_2. General procedure: 5.0 g of Fe_3O_4 nanoparticles were dispersed into 100 mL of citric acid solution (0.5 mol/L) with vigorous stirring for 2 h under a nitrogen atmosphere. The pH value of the solution was adjusted to 5.5 with NaOH (1.0 mol/L). Subsequently, 10 mL of $NH_3{\cdot}H_2O$, 5.0 mL of NaOH solution (40 wt %), and 5.0 mL of TEOS were added to the mixture under nitrogen protection. The reaction was stirred at 80 °C for 8 h. After cooling down, the products were collected using a magnet and washed at least five times with ethanol and deionized water, respectively. The purification products were dried in vacuum at 50 °C for 24 h.

4.5. Synthesis of CBD-MMIPs and MNIPs. General procedure: 1.0 mmol of CBD, 4.0 mmol of MAA, and 60 mL of acetonitrile were mixed in a 100 mL three-neck flask, and the mixture was stirred for 1 h to form the preassembly solution. Then, 1.0 g of Fe_3O_4@SiO_2, 16 mmol of EGDMA, 0.1 g of AIBN, and 0.2 g of PVP were added, and the reaction system was placed in a water bath at 60 °C for 12 h by stirring vigorously. After polymerization, the microspheres were sieved with 100 mesh screens to obtain uniform particles. CBD-MMIPs were prepared by washing the products with acetic acid and methanol (V/V = 2:8) until no CBD was detected. Subsequently, CBD-MMIPs were dried under vacuum at room temperature. MNIPs were prepared using the same process without CBD.

4.6. Adsorption Kinetics Experiments. CBD-MMIPs (0.5 g) and MNIPs (0.5 g) were added to 50 mL of CBD methanol solution (10 mg/mL), respectively, which were oscillated till equilibrium at regular time intervals from 5 min to 90 min in a constant temperature shaker at 25 °C. Then, the two polymers mentioned above were separated using a magnetic separator. The concentration of CBD in the supernatants was measured by HPLC analysis. The CBD adsorption capacity M (mg/g) for the CBD-MMIPs and MNIPs was calculated as follows

$$M = (C_1 - C_2)V/W \quad (7)$$

Where V (L) is the volume of CBD solution, C_1 (mg/L) and C_2 (mg/L) are the initial concentration and equilibrium concentration of CBD, respectively, and W (g) is the weight of the CBD-MMIPs or MNIPs.

4.7. Static Adsorption Experiment. CBD-MMIPs and MNIPs (0.5 g) were soaked in 20 mL of CBD/ethanol solution (i.e., the concentrations of CBD were 0.1−1.0 mg/L), respectively. After oscillating in a constant temperature shaker for 4 h at 25 °C, the polymers were separated by an external magnetic field. The concentration of CBD was determined by HPLC analysis.

4.8. Selectivity Experiment. The selectivity of the CBD-MMIPs was studied by comparing the adsorption capacity of CBD-MMIPs for CBD and its structural analogues (CBN, BPA, and phenol). CBD-MMIPs or MNIPs (1.0 g) were incubated with 40 mL of methanol solution and added into CBD, CBN, BPA, and phenol solutions with a concentration of 10 mg/L for each compound, respectively. An applied magnetic field was then used to separate the polymers from the solution after oscillating in a constant temperature shaker for 30 min at 25 °C. The concentration of residual target compounds was determined by HPLC analysis. To further study the performance of the competitive adsorption of the obtained CBD-MMIPs, 1.0 g of CBD-MMIPs or MNIPs was added into 40 mL of a mixed solution containing 10 mg/L of CBD, CBN, BPA, and phenol. Triplicates were prepared for all experiments, and the mean values were used for data analysis.

4.9. Reusability Experiment. After CBD was absorbed into the CBD-MMIPs or MNIPs under the optimal conditions, the CBD-MMIPs or MNIPs were eluted with the mixture solution of acetic acid: methanol (V/V = 2:8) in a constant temperature shaker for 30 min at 25 °C. Then, the adsorbent was collected under an applied magnetic field and washed with

https://doi.org/10.1021/acsomega.2c06649
ACS Omega 2023, 8, 1240−1248

ultrapure water two to three times until acid-free. After complete elution, the dried CBD-MMIPs or MNIPs were subjected to another adsorption process, and their residual adsorption capacity was assessed. This regeneration process was carried out another eight times.

4.10. Determination of CBD in Hemp Leaf Samples. General procedure: the freeze-dried hemp leaves (10 g) and 100 mL of 95% ethanol were placed in a 250 mL conical flask for reflux for 8 h. After cooling down, the extracts were filtered through a 0.22 μm filter membrane. Subsequently, CBD-MMIPs (0.1 g) were added to 20 mL of ethanol extracts and kept shaking for 40 min at 25 °C. The CBD-MMIPs were separated using a magnet and eluted with 10 mL of acetic acid: methanol (V/V = 2:8) for 30 min. Finally, the remaining eluent was evaporated to dryness and redissolved in 1.0 mL of methanol for HPLC analysis.

■ ASSOCIATED CONTENT

Supporting Information

The Supporting Information is available free of charge at https://pubs.acs.org/doi/10.1021/acsomega.2c06649.

Optimization of polymerization; N_2 adsorption−desorption isotherm and BJH pore size distribution of CBD-MMIPs and MNIPs; infrared spectrogram; XRD spectrum; adsorption kinetics and adsorption isotherm of CBD-MMIPs and MNIPs for CBD; molecular structures of CBD, CBN, BPA, and phenol; competitive adsorption; reusability of the CBD-MMIPs and MNIPs; optimization of desorption conditions (Tables S1−S4) (PDF)

■ AUTHOR INFORMATION

Corresponding Authors

Dong Fu − *Institute of Advanced Technology, Heilongjiang Academy of Sciences, Harbin 150020, China*; Email: sato2004@163.com

Bo Huang − *Institute of Advanced Technology, Heilongjiang Academy of Sciences, Harbin 150020, China*; orcid.org/0000-0003-0911-5739; Email: jingxihuagong215@163.com

Authors

Fan Yang − *Institute of Advanced Technology, Heilongjiang Academy of Sciences, Harbin 150020, China*

Peng Li − *Institute of Advanced Technology, Heilongjiang Academy of Sciences, Harbin 150020, China*

Xin Sui − *Institute of Advanced Technology, Heilongjiang Academy of Sciences, Harbin 150020, China*

Yang Xie − *Institute of Advanced Technology, Heilongjiang Academy of Sciences, Harbin 150020, China*

Jialong Chi − *Institute of Advanced Technology, Heilongjiang Academy of Sciences, Harbin 150020, China*

Jiaying Liu − *Institute of Advanced Technology, Heilongjiang Academy of Sciences, Harbin 150020, China*

Complete contact information is available at: https://pubs.acs.org/10.1021/acsomega.2c06649

Notes

The authors declare no competing financial interest.

■ ACKNOWLEDGMENTS

This work was supported by the Research and Development Fund for Smart Science Valley System of China (ZHKG2020)

■ REFERENCES

(1) Silmore, L. H.; Willmer, A. R.; Capparelli, E. V.; Rosania, G. R. Food effects on the formulation, dosing, and administration of cannabidiol (CBD) in humans: a systematic review of clinical studies. *Pharmacotherapy* **2021**, *41*, 405−420.

(2) Peng, J.; Fan, M.; An, C.; Ni, F.; et al. A narrative review of molecular mechanism and therapeutic effect of cannabidiol (CBD). *Basic Clin. Pharmacol. Toxicol.* **2022**, *130*, 439−456.

(3) Franco, V.; Bialer, M.; Perucca, E. Cannabidiol in the treatment of epilepsy: current evidence and perspectives for further research. *Neuropharmacology* **2021**, *185*, No. 108442.

(4) Chaves, Y. C.; Genaro, K.; Crippa, J. A.; da Cunha, J. M.; Zanoveli, J. M. Cannabidiol induces antidepressant and anxiolytic-like effects in experimental type-1 diabetic animals by multiple sites of action. *Metab. Brain Dis.* **2021**, *36*, 639−652.

(5) Blaskovich, M. A. T.; Kavanagh, A. M.; Elliott, A. G.; Zhang, B.; Ramu, S.; Amado, M.; Lowe, G. J.; Hinton, A. O.; Thu Pham, D. M.; Zuegg, J.; Beare, N.; Quach, D.; Sharp, M. D.; Pogliano, J.; Rogers, A. P.; Lyras, D.; Tan, L.; West, N. P.; Crawford, D. W.; Peterson, M. L.; Callahan, M.; Thurn, M. The antimicrobial potential of cannabidiol. *Commun. Biol.* **2021**, *4*, No. 7.

(6) Olivas-Aguirre, M.; Torres-López, L.; Villatoro-Gómez, K.; Perez-Tapia, S. M.; Pottosin, I.; Dobrovinskaya, O. Cannabidiol on the path from the lab to the cancer patient: opportunities and challenges. *Pharmaceuticals* **2022**, *15*, No. 366.

(7) Seltzer, E. S.; Watters, A. K.; MacKenzie, D., Jr; Granat, L. M.; Zhang, D. Cannabidiol (CBD) as a promising anti-cancer drug. *Cancers* **2020**, *12*, No. 3203.

(8) Hazekamp, A. The trouble with CBD oil. *Med. Cannabis Cannabinoids* **2018**, *1*, 65−72.

(9) Karaźniewicz-Łada, M.; Główka, A. K.; Mikulska, A. A.; Główka, F. K. Pharmacokinetic drug-drug interactions among antiepileptic drugs, including CBD, drugs used to treat COVID-19 and nutrients. *Int. J. Mol. Sci.* **2021**, *22*, No. 9582.

(10) De Vita, D.; Madia, V. N.; Tudino, V.; Saccoliti, F.; De Leo, A.; Messore, A.; Roscilli, P.; Botto, A.; Pindinello, I.; Santilli, G.; Scipione, L.; Costi, R.; Di Santo, R. Comparison of different methods for the extraction of cannabinoids from cannabis. *Nat. Prod. Res.* **2020**, *34*, 2952−2958.

(11) Brighenti, V.; Protti, M.; Anceschi, L.; Zanardi, C.; Mercolini, L.; Pellati, F. Emerging challenges in the extraction, analysis and bioanalysis of cannabidiol and related compounds. *J. Pharm. Biomed. Anal.* **2021**, *192*, No. 113633.

(12) Nelson, K. M.; Bisson, J.; Singh, G.; Graham, J. G.; Chen, S.-N.; Friesen, J. B.; Dahlin, J. L.; Niemitz, M.; Walters, M. A.; Pauli, G. F. The essential medicinal chemistry of cannabidiol (CBD). *J. Med. Chem.* **2020**, *63*, 12137−12155.

(13) Grijó, D. R.; Osorio, I. A. V.; Cardozo-Filho, L. Supercritical extraction strategies using CO_2 and ethanol to obtain cannabinoid compounds from *Cannabis* hybrid flowers. *J. CO_2 Util.* **2018**, *28*, 174−180.

(14) Marzorati, S.; Friscione, D.; Picchi, E.; Verotta, L. Cannabidiol from inflorescences of *Cannabis sativa* L.: Green extraction and purification processes. *Ind. Crops Prod.* **2020**, *155*, No. 112816.

(15) Ayankojo, A. G.; Reut, J.; Nguyen, V. B. C.; Boroznjak, R.; Syritski, V. Advances in detection of antibiotic pollutants in aqueous media using molecular imprinting technique-A Review. *Biosensors* **2022**, *12*, No. 441.

(16) Surapong, N.; Burakham, R. Magnetic molecularly imprinted polymer for the selective enrichment of glyphosate, glufosinate, and aminomethylphosphonic acid prior to high-performance liquid chromatography. *ACS Omega* **2021**, *6*, 27007−27016.

(17) Kong, X.; Li, F.; Li, Y.; He, X.; Chen, L.; Zhang, Y. Molecularly imprinted polymer functionalized magnetic Fe_3O_4 for the highly selective extraction of triclosan. *J. Sep. Sci.* **2020**, *43*, 808−817.
(18) Zhang, Y.; Xie, Y.; Zhang, C.; Wu, M.; Feng, S. Preparation of porous magnetic molecularly imprinted polymers for fast and specifically extracting trace norfloxacin residue in pork liver. *J. Sep. Sci.* **2020**, *43*, 478−485.
(19) Cheng, Y.; Nie, J.; Li, Z.; Yan, Z.; Xu, G.; Li, H.; Guan, D. A molecularly imprinted polymer synthesized using β-cyclodextrin as the monomer for the efficient recognition of forchlorfenuron in fruits. *Anal. Bioanal. Chem.* **2017**, *409*, 5065−5072.
(20) Zeng, H.; Wang, Y.; Liu, X.; Kong, J.; Nie, C. Preparation of molecular imprinted polymers using bi-functional monomer and bi-crosslinker for solid-phase extraction of rutin. *Talanta* **2012**, *93*, 172−181.
(21) Cheng, Y.; Jiang, P.; Dong, X. Molecularly imprinted fluorescent chemosensor synthesized using quinoline-modified-β-cyclodextrin as monomer for spermidine recognition. *RSC Adv.* **2015**, *5*, 55066−55074.
(22) Cheng, Y.; Jiang, P.; Lin, S.; Li, Y.; Dong, X. An imprinted fluorescent chemosensor prepared using dansyl-modified β-cyclodextrin as the functional monomer for sensing of cholesterol with tailor-made selectivity. *Sens. Actuators, B* **2014**, *193*, 838−843.
(23) Deng, D. L.; Zhang, J. Y.; Chen, C.; Hou, X. L.; Su, Y. Y.; Wu, L. Monolithic molecular imprinted polymer fiber for recognition and solid phase microextraction of ephedrine and pseudoephedrine in biological samples prior to capillary electrophoresis analysis. *J. Chromatogr. A* **2012**, *1219*, 195−200.
(24) Wulff, G. Enzyme-like catalysis by molecularly imprinted polymers. *Chem. Rev.* **2002**, *102*, 1−28.
(25) Tang, Y.; Gao, J.; Liu, X.; Lan, J.; Gao, X.; Ma, Y.; Li, M.; Li, J. Determination of ractopamine in pork using a magnetic molecularly imprinted polymer as adsorbent followed by HPLC. *Food Chem.* **2016**, *201*, 72−79.
(26) Wang, X.; Wang, L.; He, X.; Zhang, Y.; Chen, L. A molecularly imprinted polymer-coated nanocomposite of magnetic nanoparticles for estrone recognition. *Talanta* **2009**, *78*, 327−332.
(27) Chang, L.; Chen, S.; Li, X. Synthesis and properties of core-shell magnetic molecular imprinted polymers. *Appl. Surf. Sci.* **2012**, *258*, 6660−6664.
(28) Fan, D.; Li, H.; Shi, S.; Chen, X. Hollow molecular imprinted polymers towards rapid, effective and selective extraction of caffeic acid from fruits. *J. Chromatogr. A* **2016**, *1470*, 27−32.
(29) Fan, J. P.; Xu, X. K.; Xu, R.; Zhang, X. H.; Zhu, J. H. Preparation and characterization of molecular imprinted polymer functionalized with core/shell magnetic particles (Fe_3O_4@SiO_2@MIP) for the simultaneous recognition and enrichment of four taxoids in Taxus×media. *Chem. Eng. J.* **2015**, *279*, 567−577.
(30) Li, F.; Gao, J.; Li, X.; Li, Y.; He, X.; Chen, L.; Zhang, Y. Preparation of magnetic molecularly imprinted polymers functionalized carbon nanotubes for highly selective removal of aristolochic acid. *J. Chromatogr. A* **2019**, *1602*, 168−177.
(31) Xie, X.; Hu, Q.; Ke, R.; Zhen, X.; Bu, Y.; Wang, S. Facile preparation of photonic and magnetic dual responsive protein imprinted nanomaterial for specific recognition of bovine hemoglobin. *Chem. Eng. J.* **2019**, *371*, 130−137.
(32) Cheng, Y.; Nie, J.; Liu, H.; Kuang, L.; Xu, G. Synthesis and characterization of magnetic molecularly imprinted polymers for effective extraction and determination of kaempferol from apple samples. *J. Chromatogr. A* **2020**, *1630*, No. 461531.
(33) Xie, X.; Li, J.; Zhen, X.; Chen, L.; Yuan, W.; Feng, Q.; Liu, X. Rational construction of fluorescent molecular imprinted polymers for highly efficient glycoprotein detection. *Anal. Chim. Acta* **2022**, *1209*, No. 339875.
(34) Xie, X.; Liu, X.; Pan, X.; Chen, L.; Wang, S. Surface-imprinted magnetic particles for highly selective sulfonamides recognition prepared by reversible addition fragmentation chain transfer polymerization. *Anal. Bioanal. Chem.* **2016**, *408*, 693−970.
(35) Li, J.; Yang, Y.; Zhu, A.; Li, L.; Liu, X.; Xie, X. Improved detection and recognition of glycoproteins using fluorescent polymers with a molecular imprint based on glycopeptides. *Microchim. Acta* **2021**, *188*, No. 439.
(36) Zhao, Y.; Bi, C.; He, X.; Chen, L.; Zhang, Y. Preparation of molecularly imprinted polymers based on magnetic carbon nanotubes for determination of sulfamethoxazole in food samples. *RSC Adv.* **2015**, *5*, 70309−70318.
(37) Xie, X.; Chen, L.; Pan, X.; Wang, S. Synthesis of magnetic molecularly imprinted polymers by reversible addition fragmentation chain transfer strategy and its application in the sudan dyes residue analysis. *J. Chromatogr. A* **2015**, *1405*, 32−39.
(38) Ma, R. T.; Shi, Y. P. Magnetic molecularly imprinted polymer for the selective extraction of quercetagetin from *Calendula officinalis* extract. *Talanta* **2015**, *134*, 650−656.
(39) Gao, W.; Li, J.; Li, P.; Huang, Z.; Cao, Y.; Liu, X. Preparation of magnetic molecularly imprinted polymer (MMIP) nanoparticles (NPs) for the selective extraction of tetracycline from milk. *Anal. Lett.* **2020**, *53*, 1097−1112.
(40) Yuan, Y.; Liu, Y.; Teng, W.; Tan, J.; Liang, Y.; Tang, Y. Preparation of core-shell magnetic molecular imprinted polymer with binary monomer for the fast and selective extraction of bisphenol A from milk. *J. Chromatogr. A* **2016**, *1462*, 2−7.
(41) Su, X.; Li, X.; Li, J.; Liu, M.; Lei, F.; Tan, X.; Li, P.; Luo, W. Synthesis and characterization of core-shell magnetic molecularly imprinted polymers for solid-phase extraction and determination of Rhodamine B in food. *Food Chem.* **2015**, *171*, 292−297.
(42) Anirudhan, T. S.; Christa, J.; Deepa, J. R. Extraction of melamine from milk using a magnetic molecularly imprinted polymer. *Food Chem.* **2017**, *227*, 85−92.
(43) Chen, F. F.; Xie, X. Y.; Shi, Y. P. Preparation of magnetic molecularly imprinted polymer for selective recognition of resveratrol in wine. *J. Chromatogr. A* **2013**, *1300*, 112−118.
(44) Ji, Y.; Zhao, J.; Zhao, L. Fabrication and characterization of magnetic molecularly imprinted polymer based on deep eutectic solvent for specific recognition and quantification of vanillin in infant complementary food. *Food Chem.* **2022**, *374*, No. 131720.
(45) Xu, Y.; Zhao, Q.; Jiang, L.; Li, Z.; Chen, Y.; Ding, L. Selective determination of sulfonamides from environmental water based on magnetic surface molecularly imprinting technology. *Environ. Sci. Pollut. Res.* **2017**, *24*, 9174−9186.
(46) Kong, X.; Gao, R.; He, X.; Chen, L.; Zhang, Y. Synthesis and characterization of the core-shell magnetic molecularly imprinted polymers (Fe_3O_4@MIPs) adsorbents for effective extraction and determination of sulfonamides in the poultry feed. *J. Chromatogr. A* **2012**, *1245*, 8−16.

https://doi.org/10.1021/acsomega.2c06649
ACS Omega 2023, 8, 1240−1248